RESEARCH   **Open Access**

CrossMark

Convergence of an explicit iterative leap-frog discontinuous Galerkin method for time-domain Maxwell's equations in anisotropic materials

Adérito Araújo[1*] , Sílvia Barbeiro[1] and Maryam Khaksar Ghalati[2]

*Correspondence: alma@mat.uc.pt
[1]CMUC, Department of
Mathematics, University of Coimbra,
Coimbra, Portugal
Full list of author information is
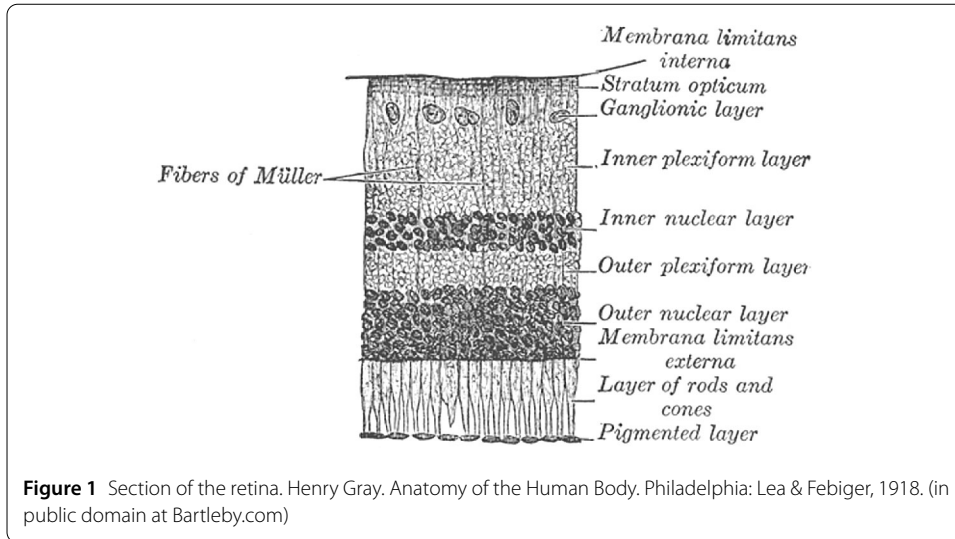available at the end of the article

Abstract

We propose an explicit iterative leap-frog discontinuous Galerkin method for time-domain Maxwell's equations in anisotropic materials and derive its convergence properties. The *a priori* error estimates are illustrated by numerical means in some experiments. Motivated by a real application which encompasses modeling electromagnetic wave's propagation through the eye's structures, we simulate our model in a 2D domain aiming to represent a simple example of light scattering in the outer nuclear layer of the retina.

Keywords: Maxwell's equations; Explicit iterative leap-frog discontinuous Galerkin method; Convergence; Light scattering

1 Introduction

The human retina is a complex structure in the eye that is responsible for the sense of vision. It is part of the central nervous system and it is composed by several layers, namely the outer nuclear layer that comprises the cells bodies of light sensitive photoreceptors cells, rods and cones (see Fig. 1) [11]. For many diseases that affect the eye, the diagnosis is not straightforward. The sensitivity of this structure makes medical analysis particularly complicated. Most of the diagnoses are made either by direct observation, with the possible injection of dyes, to enhance certain parts of the organ, or by numbing the eye and directly measuring its inner pressure or thickness. There are a number of eye-related pathologies that can be identified by the detailed analysis of the retinal layers [16].

Optical Coherence Tomography (OCT) is an increasingly popular noninvasive technique that has been successfully used as a diagnostic tool in ophthalmology in the past decades. This method allows the assessment of the human retina *in vivo* and has been shown to provide functional information. By analysing data acquired through OCT, several retinal pathologies, such as diabetic retinopathy, or macular edema, can be detected in their early stages, before noticeable morphologic alterations on the retina [16]. As OCT standard techniques only provide structural information [14], it is necessary to expand OCT data analysis to account for both structural and functional information. OCT provides also the possibility of evaluating different elements in measuring the retinal nerve

Figure 1 Section of the retina. Henry Gray. Anatomy of the Human Body. Philadelphia: Lea & Febiger, 1918. (in public domain at Bartleby.com)

fiber layer (RNFL), namely the tendency of RNFL thinning in glaucoma and other diseases that involve optic nerve atrophy. Waveguides with induced anisotropy may worth to be considered for modeling biological waveguides [10].

Maxwell's equations are a fundamental set of partial differential equations which describe electromagnetic wave interactions with materials. The electromagnetic fields in space are classically described by two field vectors, E and H, respectively electric field and magnetic field. Here we shall consider the time domain Maxwell's equations in the transverse electric mode, as in [8], where the only non-vanishing components of the electromagnetic fields are E_x, E_y and H_z. Using the following notation for the vector and scalar curl operators

$$\nabla \times H = \left(\frac{\partial H_z}{\partial y}, -\frac{\partial H_z}{\partial x} \right)^T, \quad \text{curl}\, E = \frac{\partial E_y}{\partial x} - \frac{\partial E_x}{\partial y},$$

and assuming no conductivity effects, the equations in the non-dimensional form are

$$\epsilon \frac{\partial E}{\partial t} = \nabla \times H, \qquad \mu \frac{\partial H}{\partial t} = -\text{curl}\, E, \quad \text{in } \Omega \times (0, T_f], \tag{1}$$

where $E = (E_x, E_y)^T$ represents the electric field components and $H = (H_z)$ represents the magnetic field component. These equations are set and solved on a bounded polygonal domain $\Omega \subset \mathbb{R}^2$.

The electric permittivity of the medium, ϵ, and the magnetic permeability of the medium, μ, are varying in space, being μ a scalar function and ϵ an anisotropic tensor

$$\epsilon = \begin{pmatrix} \epsilon_{xx} & \epsilon_{xy} \\ \epsilon_{yx} & \epsilon_{yy} \end{pmatrix}. \tag{2}$$

We assume that electric permittivity tensor ϵ is symmetric and uniformly positive definite for almost every $(x, y) \in \Omega$, and that it is uniformly bounded with a strictly positive lower bound, *i.e.*, there are constants $\underline{\epsilon} > 0$ and $\overline{\epsilon} > 0$ such that, for almost every $(x, y) \in \Omega$, $\underline{\epsilon} |\xi|^2 \leq$

$\xi^T \epsilon(x,y)\xi \leq \overline{\epsilon}|\xi|^2, \forall \xi \in \mathbb{R}^2$. We also assume that there are constants $\underline{\mu} > 0$ and $\overline{\mu} > 0$ such that, for almost every $(x,y) \in \Omega$, $\underline{\mu} \leq \mu(x,y) \leq \overline{\mu}$.

Equations (1) must be complemented by initial conditions $E(x,y,0) = E_0(x,y)$ and $H(x,y,0) = H_0(x,y)$, $(x,y) \in \Omega$, and by proper boundary conditions. Motivated by our application of interest, here we consider absorbing boundary conditions which mimic an open space by absorbing the incident radiation in the truncated computational domain. The first order Silver-Müller absorbing boundary conditions (SM-ABC) are defined by

$$n \times E = c\mu n \times (H \times n) \quad \text{on } \partial\Omega, \tag{3}$$

where $n = (n_x, n_y)^T$ is the unit outward normal vector to the boundary and c is the speed with which a wave travels along the direction of the unit normal, defined, using the effective permittivity $\epsilon_{\text{eff}} = \det(\epsilon)/(n^T \epsilon n)$ (see [8]), by $c = 1/\sqrt{\mu\epsilon_{\text{eff}}}$.

We can write Maxwell's equations (1) in a conservation form

$$Q\frac{\partial q}{\partial t} + \nabla \cdot F(q) = 0 \quad \text{in } \Omega \times (0, T_f], \tag{4}$$

with

$$Q = \begin{pmatrix} \epsilon & 0 \\ 0 & \mu \end{pmatrix}, \qquad q = \begin{pmatrix} E_x \\ E_y \\ H_z \end{pmatrix} \quad \text{and} \quad \nabla \cdot F(q) = \begin{pmatrix} -\frac{\partial H_z}{\partial y} \\ \frac{\partial H_z}{\partial x} \\ \frac{\partial E_y}{\partial x} - \frac{\partial E_x}{\partial y} \end{pmatrix}.$$

The attention to the development of explicit high-order accurate methods for solving time-domain Maxwell's equations in complex geometries brings to the use of discontinuous Galerkin (DG) methods with finite difference schemes for time discretization. Those methods for time-dependent Maxwell's equations are derived considering them either in first-order hyperbolic form (see, e.g. [1, 4, 7]) or alternatively in second-order form as wave equations (see, e.g. [6]). Generally, high-order explicit schemes for time discretizations require restrictive stability conditions. For these reasons, the one-step explicit time integration methods, like leap-frog schemes, are usually considered since they are computationally efficient per update cycle and easy to implement (see, e.g. [4, 5] and the references therein). The treatment of anisotropic materials within a DGTD framework was discussed for instance in [4] (with central fluxes) and in [8] (with upwind fluxes). The stability analysis of DGTD methods for Maxwell's equations was considered in [4], where the scheme that is defined with the central fluxes leads to a locally implicit time method in the case of SM-ABC, and [9], where the scheme is defined with the upwind fluxes leading to an implicit method. In [1] we extends the results in [4] and [9] to a fully explicit in time method for both cases, central fluxes and upwind fluxes. The error estimates derived therein show that the method is only first order convergent in time when SM-ABC are considered.

In the present work we propose an iterative predictor-corrector method based on the explicit method investigated in [1], resulting a fully explicit method that is second order convergent in time for the SM-ABC case. In the Sect. 2 we prove that the explicit iterative method converges to a second order in time implicit method and we deduce the *a priori* error estimates for the fully discrete scheme. In Sect. 3 we illustrate the theoretical results

with some numerical examples and, in Sect. 4, we apply the numerical method to a computational model that aims to simulate the light scattering through the outer nuclear layer of the retina.

This work was developed in the framework of a more general project that aims to develop a computational model to simulate the electromagnetic wave's propagation through the eye's structures in order to create a virtual optical coherence tomography scan [13].

2 An explicit iterative leap-frog discontinuous Galerkin method
2.1 Numerical scheme

Assume that the computational domain Ω is a bounded polygonal set that is partitioned into K triangular elements T_k such that $\overline{\Omega} = \bigcup_k T_k$. The finite element space is then taken to be $V_N = \{v \in L^2(\Omega)^3 : v|_{T_k} \in P_N(T_k)^3\}$, where $P_N(T_k)$ denotes the space of polynomials of degree less than or equal to N defined on T_k. On each element T_k, the solution fields $q_k(x, y, t) = (E_x(x, y, t), E_y(x, y, t), H_z(x, y, t))^T$ are approximated by the piecewise polynomial functions $\hat{q}_k(x, y, t) = (\hat{E}_{xk}(x, y, t), \hat{E}_{yk}(x, y, t), \hat{H}_{zk}(x, y, t))^T$.

In order to deduce the method, we start by multiplying equation (4) by test functions $v \in V_N$, usually the Lagrange polynomials, and integrate over each element T_k. The next step is to employ one integration by parts and to substitute in the resulting contour integral the flux F by a numerical flux F^*. Reversing the integration by parts yields

$$\int_{T_k} \left(Q\frac{\partial \hat{q}}{\partial t} + \nabla \cdot F(\hat{q}) \right) \cdot v(x, y) \, dx \, dy = \int_{\partial T_k} \left(n \cdot \left(F(\hat{q}) - F^*(\hat{q}) \right) \right) \cdot v(x, y) \, ds,$$

where n is the outward pointing unit normal vector of the contour.

The approximate fields are allowed to be discontinuous across element boundaries. In this way, we introduce the notation for the jumps of the field values across the interfaces of the elements, $[\hat{E}] = \hat{E}^- - \hat{E}^+$ and $[\hat{H}] = \hat{H}^- - \hat{H}^+$, where the superscript "+" denotes the neighboring element and the superscript "−" refers to the local cell. Furthermore we introduce, respectively, the cell-impedances and cell-conductances $Z^\pm = \mu^\pm c^\pm$ and $Y^\pm = (Z^\pm)^{-1}$. At the outer cell boundaries we set $Z^+ = Z^-$.

The coupling between elements is introduced via numerical flux, defined by

$$n \cdot \left(F(\tilde{q}) - F^*(\tilde{q}) \right) = \begin{pmatrix} \frac{-n_y}{Z^+ + Z^-}(Z^+[\tilde{H}_z] - \alpha(n_x[\tilde{E}_y] - n_y[\tilde{E}_x])) \\ \frac{n_x}{Z^+ + Z^-}(Z^+[\tilde{H}_z] - \alpha(n_x[\tilde{E}_y] - n_y[\tilde{E}_x])) \\ \frac{1}{Y^+ + Y^-}(Y^+(n_x[\tilde{E}_y] - n_y[\tilde{E}_x]) - \alpha[\tilde{H}_z]) \end{pmatrix}.$$

The parameter $\alpha \in [0, 1]$ in the numerical flux can be used to control dissipation. Taking $\alpha = 0$ yields a non dissipative central flux while $\alpha = 1$ corresponds to the classic upwind flux.

To define the fully discrete scheme, we divide the time interval into M subintervals by the points $0 = t^0 < t^1 < \cdots < t^M = T$, where $t^m = m\Delta t$, Δt is the time step size and $T + \Delta t/2 \leq T_f$. The unknowns related to the electric field are approximated at integer time-stations t^m and are denoted by $\hat{E}_k^m = \hat{E}_k(\cdot, t^m)$. The unknowns related to the magnetic field are approximated at half-integer time-stations $t^{m+1/2} = (m + \frac{1}{2})\Delta t$ and are denoted by $\hat{H}_k^{m+1/2} = \hat{H}_k(\cdot, t^{m+1/2})$.

With the above setting, we can now formulate the iterative leap-frog DG method. The process starts with an approximation to the initial data which we denote by $(\hat{E}_x^0,$

$\hat{E}_y^0, \hat{H}_z^{1/2})^T \in V_N$. For each $m = 0, 1, \ldots, M - 1$, we initialize the iterative process by

$$\hat{E}_x^{m+1,0} = \hat{E}_x^m, \qquad \hat{E}_y^{m+1,0} = \hat{E}_y^m, \qquad \hat{H}_z^{m+3/2,0} = \hat{H}_z^{m+1/2}.$$

The iterative scheme consists in calculating $(\hat{E}_x^{m+1}, \hat{E}_y^{m+1}, \hat{H}_{z_k}^{m+3/2})^T \in V_N$, for all $(u, v, w)^T \in V_N$, in the following way. For $n = 0, 1, 2, \ldots$, we find $\hat{E}_{x_k}^{m+1,n+1}$ and $\hat{E}_{y_k}^{m+1,n+1}$ such that

$$\left(\epsilon_{xx} \frac{\hat{E}_{x_k}^{m+1,n+1} - \hat{E}_{x_k}^m}{\Delta t} + \epsilon_{xy} \frac{\hat{E}_{y_k}^{m+1,n+1} - \hat{E}_{y_k}^m}{\Delta t}, u_k \right)_{T_k}$$
$$= \left(\partial_y \hat{H}_{z_k}^{m+1/2}, u_k \right)_{T_k}$$
$$+ \left(\frac{-n_y}{Z^+ + Z^-} \left(Z^+ [\hat{H}_z^{m+1/2}] - \alpha \left(n_x [\hat{E}_y^{[m+1/2,n]}] - n_y [\hat{E}_x^{[m+1/2,n]}] \right) \right), u_k \right)_{\partial T_k}, \tag{5}$$

$$\left(\epsilon_{yx} \frac{\hat{E}_{x_k}^{m+1,n+1} - \hat{E}_{x_k}^m}{\Delta t} + \epsilon_{yy} \frac{\hat{E}_{y_k}^{m+1,n+1} - \hat{E}_{y_k}^m}{\Delta t}, v_k \right)_{T_k}$$
$$= -\left(\partial_x \hat{H}_{z_k}^{m+1/2}, v_k \right)_{T_k}$$
$$+ \left(\frac{n_x}{Z^+ + Z^-} \left(Z^+ [\hat{H}_z^{m+1/2}] - \alpha \left(n_x [\hat{E}_y^{[m+1/2,n]}] - n_y [\hat{E}_x^{[m+1/2,n]}] \right) \right), v_k \right)_{\partial T_k}, \tag{6}$$

until the stopping criterion $\|\hat{E}^{m+1,n+1} - \hat{E}^{m+1,n}\|_{L^2(\Omega)} < tol$ is satisfied for some pre-defined small constant tol. Then the correspondent numerical solution is denoted by $(\hat{E}_{x_k}^{m+1}, \hat{E}_{y_k}^{m+1})$. In the same way, we find $\hat{H}_{z_k}^{m+3/2}$ by calculating $\hat{H}_{z_k}^{m+3/2,n+1}$, for $n = 0, 1, 2, \ldots$, such that

$$\left(\mu \frac{\hat{H}_{z_k}^{m+3/2,n+1} - \hat{H}_{z_k}^{m+1/2}}{\Delta t}, w_k \right)_{T_k}$$
$$= \left(\partial_y \hat{E}_{x_k}^{m+1} - \partial_x \hat{E}_{y_k}^{m+1}, w_k \right)_{T_k}$$
$$+ \left(\frac{1}{Y^+ + Y^-} \left(Y^+ \left(n_x [\hat{E}_y^{m+1}] - n_y [\hat{E}_x^{m+1}] \right) - \alpha [\hat{H}_z^{[m+1,n]}] \right), w_k \right)_{\partial T_k}, \tag{7}$$

until the stopping criterion $\|\hat{H}^{m+1,n+1} - \hat{H}^{m+1,n}\|_{L^2(\Omega)} < tol$ is satisfied. Here, $(\cdot, \cdot)_{T_k}$ and $(\cdot, \cdot)_{\partial T_k}$ denote the classical $L^2(T_k)$ and $L^2(\partial T_k)$ inner-products and $\hat{E}^{[m+1/2,n]}$ and $\hat{H}^{[m+1,n]}$ are the average approximations

$$\hat{E}^{[m+1/2,n]} = \frac{\hat{E}^m + \hat{E}^{m+1,n}}{2}, \qquad \hat{H}^{[m+1,n]} = \frac{\hat{H}^{m+1/2} + \hat{H}^{m+3/2,n}}{2}.$$

The SM-ABC are discretised as in [1, 5], that is, for both upwind and central fluxes, consider $\alpha = 1$ for the numerical flux at the outer boundary and $[\tilde{E}_x] = \tilde{E}_x^-$, $[\tilde{E}_y] = \tilde{E}_y^-$ and $[\tilde{H}_z] = \tilde{H}_z^-$. We want to remark that for the case $\alpha = 0$, the inner iterations change the solution only in the triangles which have boundary edges, accordingly to the discretization of the SM-ABC.

This iterative scheme may be viewed as a predictor-corrector type method of the form $P(C)^{niter}$, where P represents the predictor step (the iteration $n = 0$), C the correction steps

(iterations $n = 1, 2, \ldots$), and niter the number of correction steps needed until the stopping criteria is verified. If we consider no inner iterations (niter = 0) we obtain the explicit method considered in [1].

2.2 Convergence result

We will show that, under a suitable stability condition, the solution of the iterative predictor-corrector scheme (5)–(7) converges to the solution of the underlying implicit method. The implicit method is defined as follows: given an initial approximation $(\tilde{E}_x^0, \tilde{E}_y^0, \tilde{H}_z^{1/2})^T \in V_N$, for each $m = 0, 1, \ldots, M - 1$, we compute $(\tilde{E}_x^{m+1}, \tilde{E}_y^{m+1}, \tilde{H}_z^{m+3/2})^T \in V_N$ such that, for all $(u, v, w)^T \in V_N$,

$$
\begin{aligned}
&\left(\epsilon_{xx} \frac{\tilde{E}_{x_k}^{m+1} - \tilde{E}_{x_k}^m}{\Delta t} + \epsilon_{xy} \frac{\tilde{E}_{y_k}^{m+1} - \tilde{E}_{y_k}^m}{\Delta t}, u_k \right)_{T_k} \\
&= \left(\partial_y \tilde{H}_{z_k}^{m+1/2}, u_k \right)_{T_k} \\
&\quad + \left(\frac{-n_y}{Z^+ + Z^-} \left(Z^+ [\tilde{H}_z^{m+1/2}] - \alpha \left(n_x [\tilde{E}_y^{[m+1/2]}] - n_y [\tilde{E}_x^{[m+1/2]}] \right) \right), u_k \right)_{\partial T_k},
\end{aligned}
\tag{8}
$$

$$
\begin{aligned}
&\left(\epsilon_{yx} \frac{\tilde{E}_{x_k}^{m+1} - \tilde{E}_{x_k}^m}{\Delta t} + \epsilon_{yy} \frac{\tilde{E}_{y_k}^{m+1} - \tilde{E}_{y_k}^m}{\Delta t}, v_k \right)_{T_k} \\
&= -\left(\partial_x \tilde{H}_{z_k}^{m+1/2}, v_k \right)_{T_k} \\
&\quad + \left(\frac{n_x}{Z^+ + Z^-} \left(Z^+ [\tilde{H}_z^{m+1/2}] - \alpha \left(n_x [\tilde{E}_y^{[m+1/2]}] - n_y [\tilde{E}_x^{[m+1/2]}] \right) \right), v_k \right)_{\partial T_k},
\end{aligned}
\tag{9}
$$

$$
\begin{aligned}
&\left(\mu \frac{\tilde{H}_{z_k}^{m+3/2} - \tilde{H}_{z_k}^{m+1/2}}{\Delta t}, w_k \right)_{T_k} \\
&= \left(\partial_y \tilde{E}_{x_k}^{m+1} - \partial_x \tilde{E}_{y_k}^{m+1}, w_k \right)_{T_k} \\
&\quad + \left(\frac{1}{Y^+ + Y^-} \left(Y^+ \left(n_x [\tilde{E}_y^{m+1}] - n_y [\tilde{E}_x^{m+1}] \right) - \alpha [\tilde{H}_z^{[m+1]}] \right), w_k \right)_{\partial T_k},
\end{aligned}
\tag{10}
$$

where we consider the average approximations $\tilde{E}^{[m+1/2]}$ for $\tilde{E}^{m+1/2}$ and $\tilde{H}^{[m+1]}$ for $\tilde{H}^{m+1}$ given by

$$
\tilde{E}^{[m+1/2]} = \frac{\tilde{E}^m + \tilde{E}^{m+1}}{2}, \qquad \tilde{H}^{[m+1]} = \frac{\tilde{H}^{m+1/2} + \tilde{H}^{m+3/2}}{2}.
\tag{11}
$$

We note that the numerical solutions are defined implicitly, since the upwind fluxes involve the unknowns $\tilde{E}_x^{m+1}$, $\tilde{E}_y^{m+1}$ and $\tilde{H}_z^{m+3/2}$.

Let h_k be the diameter of the triangle $T_k \in \mathcal{T}_h$, and h be the maximum element diameter, that is, $h_k = \sup_{P_1, P_2 \in T_K} \|P_1 - P_2\|$, $h = \max_{T_k \in \mathcal{T}_h} \{h_k\}$. We assume that the mesh is regular in the sense that there exists a constant $\tau > 0$ such that for all $T_k \in \mathcal{T}_h$, $\frac{h_k}{\tau_k} \leq \tau$, where τ_k denotes the maximum diameter of a ball inscribed in T_k. It may be proved (see [12]) that, for any $u \in P_N(T_k)$, the following trace inequality holds

$$
\|u\|_{L^2(f_k)} \leq C_\tau \sqrt{(N+1)(N+2)} h_k^{-1/2} \|u\|_{L^2(T_k)},
\tag{12}
$$

where f_k is an edge of T_k and C_τ a positive constant independent of h_k and N but dependent on the shape-regularity τ.

Let us now define the difference between two successive numeric values of the electromagnetic fields by

$$\delta_n \hat{E}_{x_k}^{m+1} = \hat{E}_{x_k}^{m+1,n+1} - \hat{E}_{x_k}^{m+1,n},$$

$$\delta_n \hat{E}_{y_k}^{m+1} = \hat{E}_{y_k}^{m+1,n+1} - \hat{E}_{y_k}^{m+1,n},$$

$$\delta_n \hat{H}_{z_k}^{m+3/2} = \hat{H}_{z_k}^{m+3/2,n+1} - \hat{H}_{z_k}^{m+3/2,n},$$

for $n = 0, 1, 2, \ldots$.

We prove the following theorem by finding upper bounds for $\delta_n \hat{E}_{x_k}^{m+1}$, $\delta_n \hat{E}_{y_k}^{m+1}$ and $\delta_n \hat{H}_{z_k}^{m+3/2}$.

Theorem 1 *The solution of the iterative predictor-corrector scheme* (5)–(7) *converges to the solution of the method* (8)–(10) *provided that the stability condition of the underlying explicit method (i.e.,* (5)–(7) *taking only the iteration $n = 0$) is satisfied, that is (see* [1])

$$\Delta t < \frac{\min\{\underline{\epsilon}, \underline{\mu}\}}{\max\{C_E, C_H\}} \min\{h_k\}, \tag{13}$$

with

$$C_E = \frac{1}{2} C_{\mathrm{inv}} N^2 + C_\tau^2 (N+1)(N+2)\left(\frac{5}{2} + \frac{\alpha + \frac{1}{4}}{\min\{Z_k\}}\right),$$

$$C_H = \frac{1}{2} C_{\mathrm{inv}} N^2 + C_\tau^2 (N+1)(N+2)\left(\frac{5}{2} + \frac{\alpha + \frac{1}{2}}{\min\{Y_k\}}\right),$$

where C_τ satisfies the trace inequality (12)*, C_{inv} is a positive constant independent of h_k and N, and Z_k and Y_k denote respectively the cell-impedance Z and the cell-conductance Y inside the triangle $T_k \in \mathcal{T}_h$.*

Proof For simplicity of the prove, we consider that the mesh $\mathcal{T}_h$ is conforming.

The stability condition (13) ensures that $\|\delta_0 \hat{E}^{m+1}\|_{L^2(\Omega)}$ and $\|\delta_0 \hat{H}_z^{m+3/2}\|_{L^2(\Omega)}$ are bounded for all $m = 0, 1, \ldots, M-1$.

Let us denote by F^{int} the set of internal edges and F^{ext} the set of edges that belong to the boundary $\delta\Omega$. Let v_k be the set of indices of the neighbouring elements of T_k. For each $i \in v_k$, we consider the internal edge $f_{ik} = T_i \cap T_k$, and we denote by n_{ik} the unit normal oriented from T_i towards T_k. For each boundary edge $f_k = T_k \cap \delta\Omega$, n_k is taken to be the unitary outer normal vector to f_k.

Taking the difference of (5)–(7) between two successive iterations, $n+1$ and n, and replacing u_k, v_k and w_k by, respectively, $\delta_n \hat{E}_{x_k}^{m+1}$, $\delta_n \hat{E}_{y_k}^{m+1}$ and $\delta_n \hat{H}_{z_k}^{m+3/2}$ and summing over all elements $T_k \in \mathcal{T}_h$, we obtain

$$\sum_{T_k \in \mathcal{T}_h} \left(\epsilon \delta_n \hat{E}_k^{m+1}, \delta_n \hat{E}_k^{m+1}\right)_{T_k}$$

$$= \frac{\Delta t}{2} \sum_{f_{ik} \in F^{\mathrm{int}}} \int_{f_{ik}} \left(\frac{(n_y)_{ki}}{Z_i + Z_k}\left((n_x)_{ki} \delta_{n-1}[\hat{E}_{y_k}^{m+1}] - (n_y)_{ki} \delta_{n-1}[\hat{E}_{x_k}^{m+1}]\right)\delta_n \hat{E}_{x_k}^{m+1}\right.$$

$$+ \frac{(n_y)_{ik}}{Z_i + Z_k}\big((n_x)_{ik}\delta_{n-1}[\hat{E}_{y_i}^{m+1}] - (n_y)_{ik}\delta_{n-1}[\hat{E}_{x_i}^{m+1}]\big)\delta_n\hat{E}_{x_i}^{m+1}\bigg)\, ds$$

$$- \frac{\Delta t}{2}\sum_{f_{ik}\in F^{\text{int}}}\int_{f_{ik}}\bigg(\frac{(n_x)_{ki}}{Z_i + Z_k}\big((n_x)_{ki}\delta_{n-1}[\hat{E}_{y_k}^{m+1}] - (n_y)_{ki}\delta_{n-1}[\hat{E}_{x_k}^{m+1}]\big)\delta_n\hat{E}_{y_k}^{m+1}$$

$$+ \frac{(n_x)_{ik}}{Z_i + Z_k}\big((n_x)_{ik}\delta_{n-1}[\hat{E}_{y_i}^{m+1}] - (n_y)_{ik}\delta_{n-1}[\hat{E}_{x_i}^{m+1}]\big)\delta_n\hat{E}_{y_i}^{m+1}\bigg)\, ds$$

$$+ \frac{\Delta t}{2}\sum_{f_k\in F^{\text{ext}}}\int_{f_k}\bigg(\frac{(n_y)_k}{2Z_k}\big((n_x)_k\delta_{n-1}[\hat{E}_{y_k}^{m+1}] - (n_y)_k\delta_{n-1}[\hat{E}_{x_k}^{m+1}]\big)\delta_n\hat{E}_{x_k}^{m+1}$$

$$- \frac{(n_x)_k}{2Z_k}\big((n_x)_k\delta_{n-1}[\hat{E}_{y_k}^{m+1}] - (n_y)_k\delta_{n-1}[\hat{E}_{x_k}^{m+1}]\big)\delta_n\hat{E}_{y_k}^{m+1}\bigg)\, ds,$$

$$\sum_{T_k\in\mathcal{T}_h}\big(\mu\delta_n\hat{H}_{z_k}^{m+3/2}, \delta_n\hat{H}_{z_k}^{m+3/2}\big)_{T_k}$$

$$= -\frac{\Delta t}{2}\sum_{f_{ik}\in F^{\text{int}}}\int_{f_{ik}}\bigg(\frac{1}{Y_i + Y_k}\delta_{n-1}[\hat{H}_{z_k}^{m+3/2}]\delta_n\hat{H}_{z_k}^{m+3/2}$$

$$+ \frac{1}{Y_i + Y_k}\delta_{n-1}[\hat{H}_{zi}^{m+3/2}]\delta_n\hat{H}_{zi}^{m+3/2}\bigg)\, ds$$

$$- \frac{\Delta t}{2}\sum_{f_k\in F^{\text{ext}}}\int_{f_k}\bigg(\frac{1}{2Y_k}\delta_{n-1}[\hat{H}_{z_k}^{m+3/2}]\delta_n\hat{H}_{z_k}^{m+3/2}\bigg)\, ds.$$

Then

$$\sum_{T_k\in\mathcal{T}_h}\big(\epsilon\delta_n\hat{E}_k^{m+1}, \delta_n\hat{E}_k^{m+1}\big)_{T_k}$$

$$= \frac{\Delta t}{2}\sum_{f_{ik}\in F^{\text{int}}}\int_{f_{ik}}\bigg(\frac{(n_y)_{ki}}{Z_i + Z_k}\big((n_x)_{ki}\delta_{n-1}[\hat{E}_{y_k}^{m+1}] - (n_y)_{ki}\delta_{n-1}[\hat{E}_{x_k}^{m+1}]\big)\delta_n[\hat{E}_{x_k}^{m+1}]\bigg)\, ds$$

$$- \frac{\Delta t}{2}\sum_{f_{ik}\in F^{\text{int}}}\int_{f_{ik}}\bigg(\frac{(n_x)_{ki}}{Z_i + Z_k}\big((n_x)_{ki}\delta_{n-1}[\hat{E}_{y_k}^{m+1}] - (n_y)_{ki}\delta_{n-1}[\hat{E}_{x_k}^{m+1}]\big)\delta_n[\hat{E}_{y_k}^{m+1}]\bigg)\, ds$$

$$+ \frac{\Delta t}{2}\sum_{f_k\in F^{\text{ext}}}\int_{f_k}\bigg(\frac{(n_y)_k}{2Z_k}\big((n_x)_k\delta_{n-1}[\hat{E}_{y_k}^{m+1}] - (n_y)_k\delta_{n-1}[\hat{E}_{x_k}^{m+1}]\big)\delta_n\hat{E}_{x_k}^{m+1}$$

$$- \frac{(n_x)_k}{2Z_k}\big((n_x)_k\delta_{n-1}[\hat{E}_{y_k}^{m+1}] - (n_y)_k\delta_{n-1}[\hat{E}_{x_k}^{m+1}]\big), \delta_n\hat{E}_{y_k}^{m+1}\bigg)\, ds,$$

and

$$\sum_{T_k\in\mathcal{T}_h}\big(\mu\delta_n\hat{H}_{z_k}^{m+3/2}, \delta_n\hat{H}_{z_k}^{m+3/2}\big)_{T_k}$$

$$= -\frac{\Delta t}{2}\sum_{f_{ik}\in F^{\text{int}}}\int_{f_{ik}}\bigg(\frac{1}{Y_i + Y_k}\delta_{n-1}[\hat{H}_{z_k}^{m+3/2}]\delta_n[\hat{H}_{z_k}^{m+3/2}]\bigg)\, ds$$

$$- \frac{\Delta t}{2}\sum_{f_k\in F^{\text{ext}}}\int_{f_k}\bigg(\frac{1}{2Y_k}\delta_{n-1}[\hat{H}_{z_k}^{m+3/2}]\delta_n\hat{H}_{z_k}^{m+3/2}\bigg)\, ds.$$

So

$$\sum_{T_k \in \mathcal{T}_h} \left(\epsilon \delta_n \hat{E}_k^{m+1}, \delta_n \hat{E}_k^{m+1} \right)_{T_k}$$

$$\leq \frac{\Delta t}{4 \min\{Z_k\}} \sum_{f_{ik} \in F^{\text{int}}} \left\| \delta_{n-1} [\hat{E}_k^{m+1}] \right\|_{L^2(f_{ik})} \left\| \delta_n [\hat{E}_k^{m+1}] \right\|_{L^2(f_{ik})}$$

$$+ \frac{\Delta t}{4 \min\{Z_k\}} \sum_{f_k \in F^{\text{ext}}} \left\| \delta_{n-1} [\hat{E}_k^{m+1}] \right\|_{L^2(f_k)} \left\| \delta_n [\hat{E}_k^{m+1}] \right\|_{L^2(f_k)},$$

$$\sum_{T_k \in \mathcal{T}_h} \left(\mu \delta_n \hat{H}_{z_k}^{m+3/2}, \delta_n \hat{H}_{z_k}^{m+3/2} \right)_{T_k}$$

$$\leq \frac{\Delta t}{4 \min\{Y_k\}} \sum_{f_{ik} \in F^{\text{int}}} \left\| \delta_{n-1} [\hat{H}_{z_k}^{m+3/2}] \right\|_{L^2(f_{ik})} \left\| \delta_n [\hat{H}_{z_k}^{m+3/2}] \right\|_{L^2(f_{ik})}$$

$$+ \frac{\Delta t}{4 \min\{Y_k\}} \sum_{f_k \in F^{\text{ext}}} \left\| \delta_{n-1} [\hat{H}_{z_k}^{m+3/2}] \right\|_{L^2(f_k)} \left\| \delta_n \hat{H}_{z_k}^{m+3/2} \right\|_{L^2(f_k)}.$$

Consequently, considering (12), we obtain

$$\underline{\epsilon} \left\| \delta_n \hat{E}^{m+1} \right\|_{L^2(\Omega)}$$

$$\leq \frac{\Delta t}{\min\{Z_k\}} C_\tau^2 (N+1)(N+2) \max\{h_k^{-1}\} \left\| \delta_{n-1} \hat{E}^{m+1} \right\|_{L^2(\Omega)},$$

$$\underline{\mu} \left\| \delta_n \hat{H}_{z_k}^{m+3/2} \right\|_{L^2(\Omega)}$$

$$\leq \frac{\Delta t}{\min\{Y_k\}} C_\tau^2 (N+1)(N+2) \max\{h_k^{-1}\} \left\| \delta_{n-1} \hat{H}_z^{m+3/2} \right\|_{L^2(\Omega)}.$$

Taking the following condition into account (that results from (13))

$$\Delta t < \frac{\min\{\underline{\epsilon}, \underline{\mu}\} \min\{Z_k, Y_k\}}{C_\tau^2 (N+1)(N+2)} \min\{h_k\},$$

we conclude that the sequences of general terms $\|\delta_n \hat{E}^{m+1}\|_{L^2(\Omega)}$ and $\|\delta_n \hat{H}_{z_k}^{m+3/2}\|_{L^2(\Omega)}$, $n = 0, 1, \ldots$, are decreasing and converge to 0. Then, the limit solution, as n tends to the infinity, of the iterative predictor-corrector scheme (5)–(7) converges to the unique solution of the method (8)–(10). □

From the proof of the previous theorem, if (13) is satisfied, we have that

$$\left\| \delta_n \hat{E}^{m+1} \right\|_{L^2(\Omega)} \leq (C_*)^n \left\| \delta_0 \hat{E}^{m+1} \right\|_{L^2(\Omega)}$$

and

$$\left\| \delta_n \hat{H}_{z_k}^{m+3/2} \right\|_{L^2(\Omega)} \leq (C_*)^n \left\| \delta_0 \hat{H}_z^{m+3/2} \right\|_{L^2(\Omega)},$$

where C_* is dependent on the material properties ϵ and μ, on the properties of the space discretization namely N and h and on the time step Δt,

$$C_* = \frac{\Delta t C_\tau^2 (N+1)(N+2)}{\min\{\underline{\epsilon}, \underline{\mu}\} \min\{Z_k, Y_k\} \min\{h_k\}} < 1.$$

For a given m, it is possible to have an estimate for the number of inner iterations needed to satisfy the stopping criterion defined by tol, considering the approximation

$$C_* \simeq \max \left\{ \frac{\|\delta_1 \hat{E}^{m+1}\|_{L^2(\Omega)}}{\|\delta_0 \hat{E}^{m+1}\|_{L^2(\Omega)}}, \frac{\|\delta_1 \hat{H}_{z_k}^{m+3/2}\|_{L^2(\Omega)}}{\|\delta_0 \hat{H}_{z_k}^{m+3/2}\|_{L^2(\Omega)}} \right\},$$

and so

$$\text{niter} \simeq \left\lceil \log\big(\text{tol} \big\| \delta_0 \hat{E}^{m+1} \big\|_{L^2(\Omega)}^{-1}\big) / \log(C_*) \right\rceil.$$

The next theorem establishes that the implicit method is second order convergent in time and arbitrary high order in space. So, with the previous result, we may conclude that, if a sufficient number of inner iterations is performed, i.e, if niter is sufficiently large, the iterative predictor-corrector scheme has, in practice, similar convergence properties.

Theorem 2 *Let us consider the implicit leap-frog DG method* (8)–(10) *complemented with the discrete boundary conditions defined in Sect.* 2.1 *and suppose that the solution of the Maxwell's equations* (1) *complemented by* (3) *has the following regularity*: $E_x, E_y, H_z \in L^\infty(0, T_f; H^{s+1}(\Omega))$, $\frac{\partial E_x}{\partial t}, \frac{\partial E_y}{\partial t}, \frac{\partial H_z}{\partial t} \in L^2(0, T_f; H^{s+1}(\Omega) \cap L^\infty(\partial\Omega))$ *and* $\frac{\partial^2 E_x}{\partial t^2}, \frac{\partial^2 E_y}{\partial t^2}, \frac{\partial^2 H_z}{\partial t^2} \in L^2(0, T_f; H^1(\Omega))$, $s \geq 0$. *If the time step* Δt *satisfies*

$$\Delta t < \frac{\min\{\underline{\epsilon}, \underline{\mu}\}}{\frac{1}{2} C_{\text{inv}} N^2 + 2 C_\tau^2 (N+1)(N+2)} \min\{h_k\}, \tag{14}$$

where C_{inv} *and* C_τ *are the positive constants defined in the previous theorem, then*
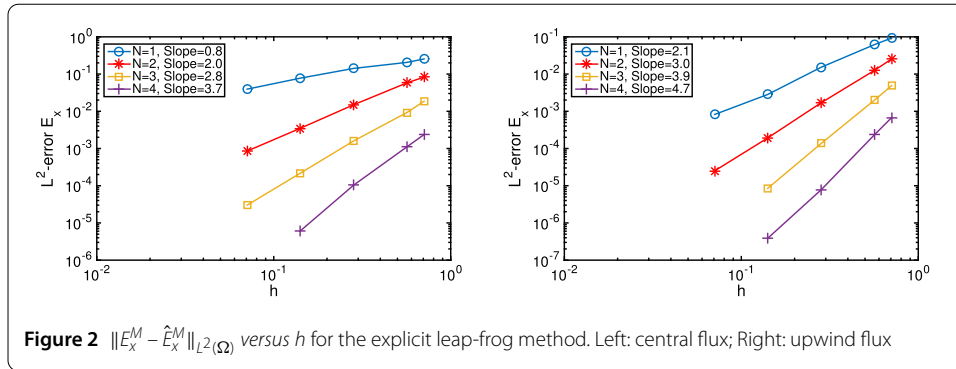
$$\max_{1 \leq m \leq M} \left(\big\| E^m - \tilde{E}^m \big\|_{L^2(\Omega)} + \big\| H_z^{m+1/2} - \tilde{H}_z^{m+1/2} \big\|_{L^2(\Omega)} \right)$$

$$\leq C\big(\Delta t^2 + h^{\min\{s, N\}}\big)$$

$$+ C\big(\big\| E^0 - \tilde{E}^0 \big\|_{L^2(\Omega)} + \big\| H_z^{1/2} - \tilde{H}_z^{1/2} \big\|_{L^2(\Omega)} \big)$$

holds, where C *is a generic positive constant independent of* Δt *and the mesh size* h.

Proof Follows the steps of the proof of Theorem 4.2 in [1]. □

3 Numerical results and discussion

To illustrate the theoretical results of the previous section, we consider the model problem (1) defined in the square $\Omega = (-1, 1)^2$, complemented by initial conditions and SM-ABC (3). In order to make it easier to find examples with known exact solution and consequently with the possibility to compute the error of the numerical solution, source terms were introduced in the model. The simulation time is fixed at $T = 1$ and in all tests we set

Figure 2 $\|\tilde{E}_x^M - \hat{E}_x^M\|_{L^2(\Omega)}$ *versus h for the explicit leap-frog method. Left: central flux; Right: upwind flux*

$\mu = 1$ and ϵ is given by (2), with $\epsilon_{xx} = 4x^2 + y^2 + 1$, $\epsilon_{yy} = x^2 + 1$ and $\epsilon_{xy} = \epsilon_{yx} = \sqrt{x^2 + y^2}$. The source terms are defined in such way that the problem has the exact solution

$$E_x(x, y, t) = -\sqrt{\frac{\epsilon_{yy}}{\det(\epsilon)}} \sin(\pi t) \sin(\pi x),$$

$$E_y(x, y, t) = \sqrt{\frac{\epsilon_{xx}}{\det(\epsilon)}} \sin(\pi t) \sin(\pi y),$$

$$H_z(x, y, t) = \sin(\pi t) \sin(\pi xy).$$

To illustrate the order of convergence in space, we fix $\Delta t = 10^{-5}$, except when $N = 4$ where we consider $\Delta t = 10^{-6}$. In Fig. 2 we plot the discrete L^2-error of the $\tilde{E}_x$ component of electric field for the explicit leap-frog method depending on the maximum element diameter of each mesh, for different degrees for the polynomial approximation, for both central and upwind fluxes. The vertical and horizontal axis are scaled logarithmically. The numerical convergence rate is approximated by the slope of the linear regression line. For central flux, the numerical convergence rate is close to the value estimated in Theorem 2, $\mathcal{O}(h^N)$, and for upwind flux we observe higher order of convergence, up to $\mathcal{O}(h^{N+1})$ in some cases. Similar results were obtained for $\tilde{E}_y$ and $\tilde{H}_z$.

To visualize the convergence order in time, the polynomial degree and the number of elements have been set to $N = 8$ and $K = 800$, respectively. The results plotted in Fig. 3 illustrate the first order convergency in time for the explicit leap-frog method and show that the second order is recovered when the predictor-corrector method is considered with just one correction step: scheme $P(C)^1$. These results correspond to upwind fluxes. The experiments using central fluxes show analogous results in terms of order of convergence in time.

In all the experiments we performed we have observed that second order convergence in time is achieved with only one correction step of the method. So, in practice, it is more efficient to consider only one inner iteration instead of doing enough inner iterations until a certain prescribed tolerance tol is achieved.

4 Modeling scattered electromagnetic wave's propagation through eye's structures

This work is part of a research project which aims to develop a cellular model of the human retina able to simulate different retinal/cellular conditions and how these changes are translated to an Optical Coherence Tomography scan [13]. Simulating the full complexity

Figure 3 $\|E_x^M - \hat{E}_x^M\|_{L^2(\Omega)}$, $\|E_y^M - \hat{E}_y^M\|_{L^2(\Omega)}$ and $\|H_z^M - \hat{H}_z^M\|_{L^2(\Omega)}$ *versus* Δt. Left: explicit leap-frog method; Right: predictor-corrector leap-frog method P(C)[1] (just one correction step)
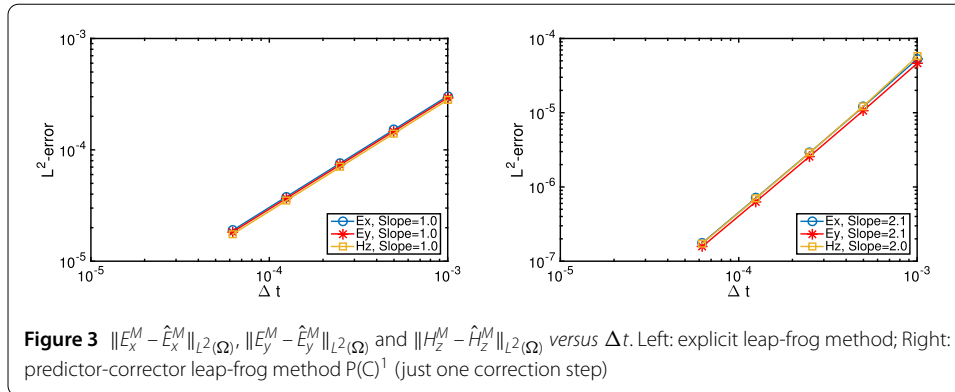
of the retina, in particular the variation of the size and shape of each structure, distance between them and the respective refractive indexes, requires a rigorous approach that can be achieved by solving Maxwell's equations. As the interest is to acquire the backscattered light intensity, we start this section by the scattered field formulation. Then we build up a two dimensional model which tries to represent a single nucleus of the outer nuclear layer (ONL) of the retina. The performance of our method is examined by simulating the light scattering in this 2D domain. The evolution of the scattering field intensity in time is obtained using the predictor-corrector DG method.

4.1 Optical coherence tomography

Optical Coherence Tomography (OCT) its an imaging technology that produces high-resolution cross-sectional images of the internal microstructure of living tissue, widely used in ophthalmological exams. This technology's working principle is analogous to ultrasound, but it uses light instead of sound to locate subtle differences in the tissue being analysed. Discontinuities in the refractive index of the tissue give rise to light scattering, with some light backscattered to the detector. Factors such as the shape and size of the scatterer, wavelength of the incident light and refractive index differences have an impact on the amount of backscattered light. During a scan, the OCT machine directs a light beam into the retina and extracts, through interferometry, the backscattered light intensity of retinal structures and their depth location in an A-scan (see Fig. 4). By transversely moving the light beam, several A-scans can be collected into a cross-sectional image – a B-scan. Usually, several cross- sectional images are acquired by probing an azimuthal direction and combined into a volume.
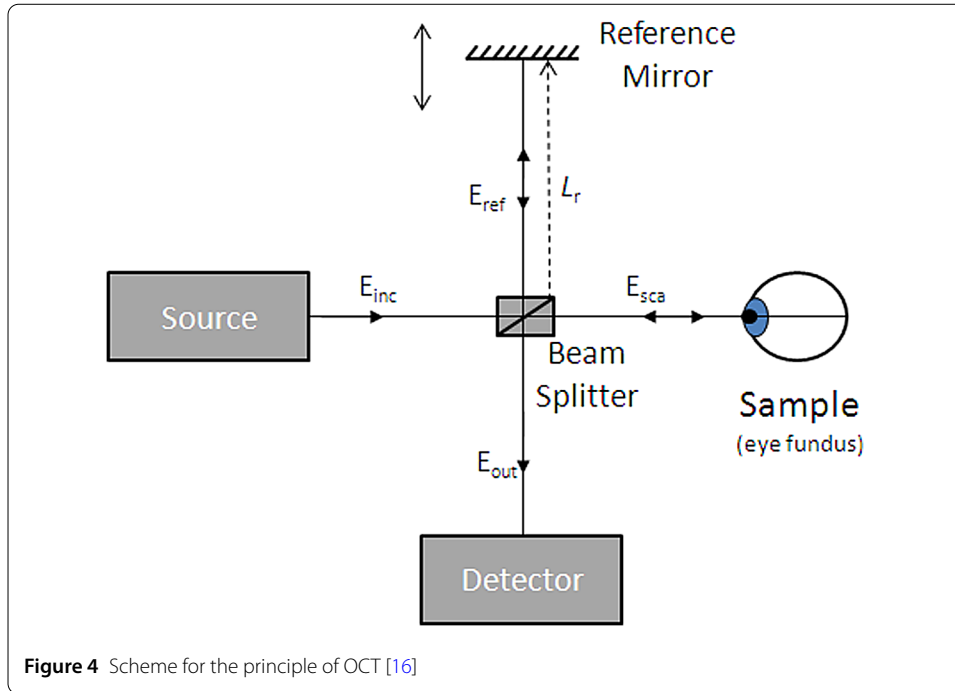
4.2 The scattered field formulation

We can exploit the linearity of the Maxwell's equations in order to separate the electromagnetic fields (E, H) into incident fields (E^i, H^i) and scattered components (E^s, H^s), *i.e.*, $E = E^s + E^i$ and $H = H^s + H^i$.

Assuming that the incident field is also a solution of the Maxwell's equations we obtain in the same way as in [17], the scattered field formulation,

$$\epsilon_{xx}\frac{\partial E_x^s}{\partial t} + \epsilon_{xy}\frac{\partial E_y^s}{\partial t} = \frac{\partial H_z^s}{\partial y} + P, \tag{15}$$

$$\epsilon_{yx}\frac{\partial E_x^s}{\partial t} + \epsilon_{yy}\frac{\partial E_y^s}{\partial t} = -\frac{\partial H_z^s}{\partial x} + Q, \tag{16}$$

Figure 4 Scheme for the principle of OCT [16]

$$\mu \frac{\partial H_z^s}{\partial t} = -\frac{\partial E_y^s}{\partial x} + \frac{\partial E_x^s}{\partial y} + R, \quad \text{in } \Omega \times (0, T], \tag{17}$$

with the source terms

$$P(x, y, t) = \left(\epsilon^i - \epsilon_{xx}\right) \frac{\partial E_x^i}{\partial t} - \epsilon_{xy} \frac{\partial E_y^i}{\partial t}, \tag{18}$$

$$Q(x, y, t) = -\epsilon_{yx} \frac{\partial E_x^i}{\partial t} + \left(\epsilon^i - \epsilon_{yy}\right) \frac{\partial E_y^i}{\partial t}, \tag{19}$$

$$R(x, y, t) = \left(\mu^i - \mu\right) \frac{\partial H_z^i}{\partial t}, \tag{20}$$

where ϵ^i and μ^i represent, respectively, the relative permittivity and permeability of the medium in which the incident field propagates in the absence of scatterers (in the background medium). Additionally, using this formulation it is straightforward to specify an incident wave using an analytic formula.

The intensity of the light that hits the OCT detector defines the output signal. Hence, we are interested in computing the scattered field intensity,

$$I^s = \sqrt{\left(E_x^s\right)^2 + \left(E_y^s\right)^2}. \tag{21}$$

4.3 Light scattering in the outer nuclear layer

We use our numerical model to simulate light scattering in the ONL. This layer has a special relevance among the retina's layers as it consistently presents the characteristics of diabetic macular edema [2, 3]. The ONL is mostly populated by the cells bodies of light sensitive photoreceptor cells (rods and cons). Thus, we postulate that the main contribution to light scattering in this layer comes from the nucleus [15], as it is the biggest

Figure 5 Square computational domain $\bar{\Omega} = [-1, 1]^2$ and the triangular mesh used in the computations: one circle (left); three circles (right)
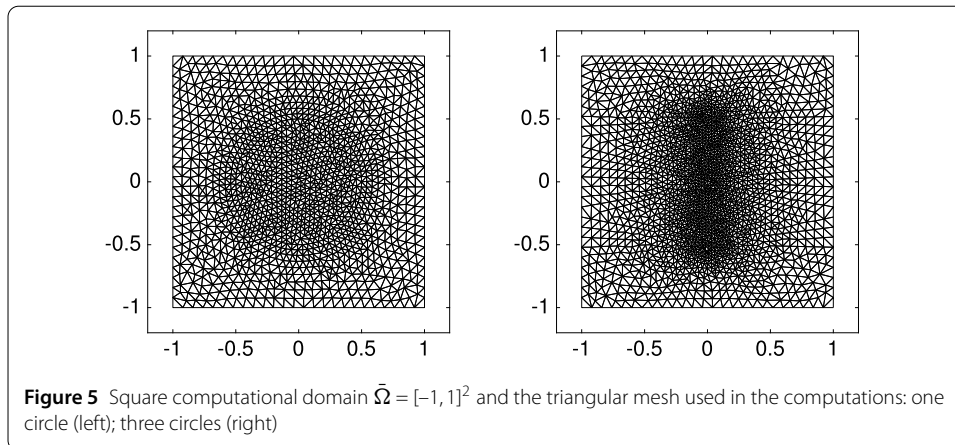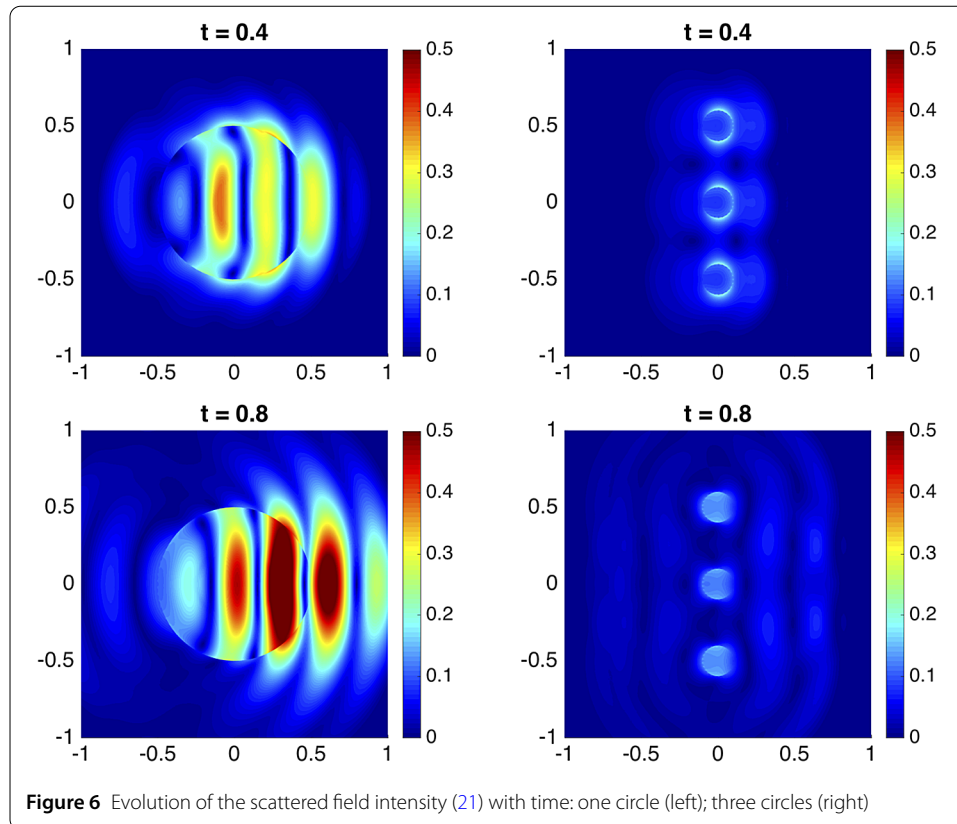
organelle in the soma and presents a high refractive index difference to the surrounding medium. As such, the ONL can be modelled as a population of spherical nuclei in an homogenous medium. As a proof of concept we present a simple simulation in a two dimensional square domain which contains circles that aims to represent, respectively, a single nucleus and three nuclei in the ONL. The permittivity inside the circles and in the background domain has different values.

Let us consider equations (15)–(17), in $\Omega = (-1, 1)^2$, complemented with SM-ABC and null initial conditions. The absorbing boundary conditions are chosen for the model as they avoid undesirable reflections that invade the computational domain. In the first experiment we will consider the case of just one circle: $\mathcal{C} = \{(x, y) \in \Omega : x^2 + y^2 < 0.25\}$. In the second example we will consider the case of three circles: $\mathcal{C}_1 = \{(x, y) \in \Omega : x^2 + (y - 0.5)^2 < 0.01\}$; $\mathcal{C}_2 = \{(x, y) \in \Omega : x^2 + y^2 < 0.01\}$; $\mathcal{C}_3 = \{(x, y) \in \Omega : x^2 + (y + 0.5)^2 < 0.01\}$. In the experiments the relative permittivity and permeability and magnetic permeability are considered as constants, $\epsilon^i = 1$ and $\mu^i = \mu = 1$. The electric permittivity is considered as a diagonal matrix with $\epsilon_{xx}(x, y) = \epsilon_{yy}(x, y) = 1.2$ for (x, y) inside the circles and $\epsilon_{xx}(x, y) = \epsilon_{yy}(x, y) = 1$ otherwise. For the incident wave we consider the planar wave $E^i_y(x, t) = \cos(10(x - t))$.

For the simulation we used with predictor-corrector DG method defined in Sect. 2 with just one correction step (scheme $P(C)^1$), considering $\alpha = 0$ (central flux) and the approximation polynomial degree $N = 4$. The time step was chosen to be $\Delta t = 0.002$ and the final simulation time is $T = 0.8$. The meshes are illustrated in Fig. 5. The evolution in time of the scattered field intensity (21) is plotted in Fig. 6. These results show that the scatterers are clearly identified. With this model, we can simulate more complex cellular structures only by changing the electric permittivity tensor ϵ.

5 Conclusions

We presented an iterative explicit leap-frog DG method for time dependent Maxwell's equations in anisotropic media, considering SM-ABC. The numerical scheme is fully explicit and converges to a second order in time implicit method. The results of a set of numerical experiments support the theoretical results and show that the second order of convergency is achieved for any number of inner iterations $n \geq 1$. Moreover we developed a 2D model which simulates the light scattering by a single nucleus in the outer nuclear layer of the retina. This work was elaborated in the framework of a more general project with a real application (see [3, 13]).

Figure 6 Evolution of the scattered field intensity (21) with time: one circle (left); three circles (right)

Abbreviations
DG, discontinuous Galerkin; OCT, optical coherence tomography; ONL, outer nuclear layer; RNFL, retinal nerve fiber layer; SM-ABC, Silver–Müller absorbing boundary conditions.

Availability of data and materials
Please contact the corresponding author for data requests.

Competing interests
The authors declare that they have no competing interests.

Authors' contributions
All authors contributed equally to the writing of this paper. All authors read and approved the final manuscript.

Author details
[1]CMUC, Department of Mathematics, University of Coimbra, Coimbra, Portugal. [2]Centre for Rapid and Sustainable Product Development, Polytechnic Institute of Leiria, Marinha Grande, Portugal.

Publisher's Note
Springer Nature remains neutral with regard to jurisdictional claims in published maps and institutional affiliations.

References
1. Araújo A, Barbeiro S, Ghalati MK. Stability of a leap-frog discontinuous Galerkin method for time-domain Maxwell's equations in anisotropic materials. Commun Comput Phys. 2017;21(5):1350–75.

2. Ciulla T, Amador A, Zinman B. Diabetic retinopathy and diabetic macular edema. Diabetes Care. 2003;26(9):2653–64.

3. Correia A, Pinto L, Araújo A, Barbeiro S, Caramelo F, Menezes P, Morgado M, Serranho P, Bernardes R. Monte Carlo simulation of diabetic macular edema changes on optical coherence tomography data. In: IEEE-EMBS international conference on biomedical and health informatics (BHI). 2014. p. 724–7.

4. Fezoui L, Lanteri S, Lohrengel S, Piperno S. Convergence and stability of a discontinuous Galerkin time-domain method for the 3D heterogeneous Maxwell's equations on unstructured meshes. ESAIM: Math Model Numer Anal. 2005;39(6):1149–76.

5. González JA. A Discontinuous Galerkin Finite Element Method for the Time-Domain Solution of Maxwell Equations. PhD thesis. Universidad de Granada, España; 2014.

6. Grote MJ, Mitkova T. Explicit local time-stepping methods for Maxwell's equations. J Comput Appl Math. 2010;234(12):3283–302.

7. Hesthaven JS, Warburton T. Nodal discontinuous Galerkin methods: algorithms, analysis, and applications. New York: Springer; 2008.

8. König M, Busch K, Niegemann J. The discontinuous Galerkin time-domain method for Maxwell's equations with anisotropic materials. Photonics Nanostruct Fundam Appl. 2010;8(4):303–9.

9. Li J, Waters JW, Machorro EA. An implicit leap-frog discontinuous Galerkin method for the time-domain Maxwell's equations in metamaterials. Comput Methods Appl Mech Eng. 2012;223–224:43–54.

10. Limeres J, Calvo ML, Enoch JM, Lakshminarayanan V. Light scattering by an array of birefringent optical waveguides: theoretical foundations. J Opt Soc Am B. 2003;20(7):1542–9.

11. Mescher AL, Junqueira LCU. Junqueira's basic histology: text and atlas. 13th ed. New York: McGraw Hill Medical; 2013.

12. Riviére B. Discontinuous Galerkin methods for solving elliptic and parabolic equations: theory and implementation. Philadelphia: SIAM; 2008.

13. Santos M, Araújo A, Barbeiro S, Caramelo F, Correia A, Marques MI, Pinto L, Serranho P, Bernardes R, Morgado M. Simulation of cellular changes on optical coherence tomography of human retina. In: 37th annual international conference of the IEEE engineering in medicine and biology society. vol. EMBC. 2015. p. 8147–50.

14. Schliesser JA, Gallimore G, Kunjukunju N, Sabates NR, Koulen P, Sabates FN. Clinical application of optical coherence tomography in combination with functional diagnostics: advantages and limitations for diagnosis and assessment of therapy outcome in central serous chorioretinopathy. Clin Ophthalmol. 2014;8:2337–45.

15. Seet KY, Nieminen TA, Zvyagin AV. Refractometry of melanocyte cell nuclei using optical scatter images recorded by digital Fourier microscopy. J Biomed Opt. 2009;14(4):044031.

16. Serranho P, Morgado M, Bernardes R. Optical coherence tomography: a concept review. In: Optical coherence tomography: a clinical and technical update. Berlin: Springer-Verlag; 2012. p. 139–56.

17. Taflove A. Computational electrodynamics: the finite-difference time-domain method. Boston: Artech House; 1995.